Minerals Engineering 234 (2025) 109682

Contents lists available at ScienceDirect

Minerals Engineering

journal homepage: www.elsevier.com/locate/mineng

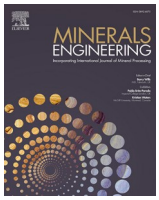

# Investigating mineral composition of PGE low-grade ore in Bushveld igneous complex, South Africa☆

Viwe Notole [a,b,c,*], Glen T. Nwaila [b,*], Mehdi Safari [b,d,*], Sehliselo Ndlovu [a,e]

[a] School of Chemical and Metallurgical Engineering, University of the Witwatersrand, 1 Jan Smuts Ave., Johannesburg 2000, South Africa
[b] African Research Centre for Ore Systems Science (CORES), School of Geosciences, University of the Witwatersrand, 1 Jan Smuts Ave., Johannesburg 2000, South Africa
[c] Wits Mining Institute, Real-time Information Management Systems (RTIMS) Research Centre, University of the Witwatersrand, 1 Jan Smuts Ave., Johannesburg 2000, South Africa
[d] Minerals Processing Division, Mintek, Private Bag X3015, Randburg 2125, South Africa
[e] School of Mining Engineering and Mineral Resources, The University of Arizona, Tucson, AZ 85721, USA

ARTICLE INFO

*Keywords:*
Bushveld igneous complex
Platinum group elements
Hyperspectral imaging
Automated mineralogy
Portable X-ray fluorescence
Geometallurgy

ABSTRACT

The mineralogically complex and low-grade ores from the 2.055 Ga Bushveld Igneous Complex (BIC) require extensive characterisation prior to beneficiation. This study integrates multi-complementary mineralogical instruments to systematically characterise Merensky Reef drill core; validates hyperspectral imaging (HSI) and portable X-ray Fluorescence (pXRF) data against reputable methods for real-time, high-throughput ore characterisation. We further evaluate the potential of pXRF in identifying high-grade platinum group elements (PGEs) zones using base metals as geochemical proxies. The HSI results using long-wave infrared, indicate that the ore predominantly comprises pyroxene (i.e., with orthopyroxene dominant over clinopyroxene), plagioclase (i.e., anorthite), olivine, and minor quartz, along with alteration minerals such as serpentine, prehnite, amphibole, talc, chlorite, and epidote. The pXRF geochemical data reveal variations in base metals with drill core depth; with higher base metal concentrations in noritic rocks compared to anorthosite. The results suggest that pXRF can be used as a tool to predict PGE high-grade zones within the drill core (with base metals as proxies). X-ray diffraction (XRD) and TESCAN Integrated Mineral Analyzer (TIMA) results confirm that the ore primarily comprises pyroxene, plagioclase, alteration minerals and base metal sulphides (BMS). The dominant BMS phases in the core samples are pentlandite, chalcopyrite, and pyrrhotite, with similar bulk mineralogical assemblages. These BMS minerals are well liberated and fine-grained, with over 40 wt% having equivalent circular diameters (ECD) between 10–38 μm. Mineral Liberation Analyzer analysis further supports these results. PGEs are primarily associated with BMS attached to silicates. The primary modes of occurrence for PGEs in the ore include PtBiTe, PtFe, PtS, and PtPdS. Most identified PGEs are fine grained with ECDs ranging between 0.6–10.97 μm. Very few PGE grains are >10.97 μm. The integration of rapid data acquisition techniques (HSI and pXRF) with automated mineralogy provides a reliable, near real-time approach for ore characterisation enabling strategic ore blending and selection of suitable processing routes. This multi-technique approach holds significant potential for improving mineral characterisation accuracy, advancing geometallurgical applications, beneficiation processes and ultimately offering a low-cost efficient pathway for selective mining.

## 1. Introduction

South Africa has a rich and extensive history of mining and metallurgical processing of valuable minerals. It stands as the repository of the world's most abundant mineral resources (Hamann, 2004; McCarthy and Rubidge, 2013). South Africa has diverse minerals that includes PGEs, chrome (Cr), nickel (Ni), gold (Au), vanadium (V), manganese (Mn), diamonds, and coal. Notably, the Bushveld Igneous Complex (BIC) is globally commended for hosting the largest deposits of PGEs, Cr, and V (McDonald et al., 2017; Mudd et al., 2018; Taguta et al., 2023). The

☆ This article is part of a special issue entitled: 'Critical Minerals'24' published in Minerals Engineering.

* Corresponding authors.
*E-mail addresses:* 1964355@students.wits.ac.za (V. Notole), glen.nwaila@wits.ac.za (G.T. Nwaila), MehdiS@Mintek.co.za (M. Safari), ndlovus@arizona.edu (S. Ndlovu).

https://doi.org/10.1016/j.mineng.2025.109682
Received 21 March 2025; Received in revised form 1 August 2025; Accepted 3 August 2025
Available online 8 August 2025

mining industry has an important role in both the production of these metals and the economic development of the country. However, in the past few decades there has been a depletion of high-grade resources (Mitra, 2019). This necessitates mining and processing of low-grade ores and mine waste or tailing material. The mining industry generates significant amount of waste, encompassing waste rocks, topsoil, and tailings (Das et al., 2024). Mine waste or tailing material from tailing dames typically contains low grades of precious metals (Mudd et al., 2018). These low-grade materials, although challenging to process, present an opportunity for PGE recovery through innovative and advanced mineral processing methods. Mineral processing offers a systematic approach for characterising low-grade orebodies and tailing material to identify suitable processing pathways and predict their potential behaviour during treatment (Wills and Finch, 2015; Nwaila et al., 2022; Baloyi et al., 2024). This study aims to systematically characterise the low-grade Merensky Reef ore using multi-complementary mineralogical instruments; validate HSI and pXRF data against traditional mineralogical methods (e.g., XRD and TIMA). We further evaluate the potential of pXRF in identify high-grade PGE zones using base metals as geochemical proxies.

Mineralogy is the basis of informed and effective decision-making throughout the mining value chain, providing important perspective into the composition, distribution, and behavior of minerals within an orebody (Dominy et al., 2018). Mineralogy supports efficient exploration by enabling accurate identification and classification of ore and gangue minerals (Cook et al., 2017; Roonwal, 2018; Carelse et al., 2022; Balaram and Sawant, 2022). It helps in resource estimation and informs mine planning by mapping mineral distribution and predicting processing performance. It informs the beneficiation technique selection downstream, allowing for tailored reagent use and separation of valuable minerals. Lastly, ore mineralogy can directly influence metal extraction rates during beneficiation (Safari et al., 2017; Ghorbani et al., 2023; Oyinloye, 2024).

The extraction and metallurgical processing of PGEs is important due to their strategic importance in various industries, including automotive (catalytic converters), electronics, jewellery, and renewable energy technologies like hydrogen fuel cells (Hughes et al., 2021). As rare and highly valuable metals, PGEs demand efficient extraction methods. The depletion of high-grade PGE ores has further introduced significant challenges in mining and minerals industry. The mining industry is increasingly forced to process low-grade ores, which are more difficult to treat (Mudd et al., 2018; Corin et al., 2021; Sahu et al., 2021). Low-grade ores require more complex and energy-intensive methods to achieve economical acceptable recovery (Gibson et al., 2023; Buchspies et al., 2017). Processing of low-grade ores often result in higher operational costs, greater environmental impacts, and reduced profitability. PGEs are often associated with complex mineral matrices, complicating the separation of valuable minerals from the surrounding gangue (McCall, 2016).

The imperative for sustainable resource utilisation in the mining sector has led to the exploration of inventive methods to extract valuable elements/minerals from low-grade ores (Gibson et al., 2023; Hu et al., 2024). Advanced technologies like automated mineralogy, Hyperspectral imaging (HSI), and machine learning are becoming essential for optimising PGE recovery from low-grade ores (Mashaba, 2022; Hrstka et al., 2018). These tools enable better ore characterisation, tailored ore processing (e.g., flotation) and help to address the challenges posed by declining ore grades and the scarcity of high-grade resources.

Despite advances in mineral characterisation techniques, significant knowledge gap remains in understanding the complex mineralogical composition of low-grade ores and its impact on flotation or leaching efficiency for PGEs recovery (Nayak et al., 2022; Sahu et al., 2021). Current methods, including X-ray diffraction (XRD), TESCAN Integrated Mineral Analyzer (TIMA) and Mineral Liberation Analyzer (MLA) provide valuable insights into mineral distribution and associations (Aylmore, 2019). However, these techniques often struggle to accurately capture the subtle variations in mineral textures and associations for large samples. These conventional mineralogy techniques require long sample preparation and processing time (Lotter, 2011; Schouwstra and Smit, 2011). As a result, there is a growing need for near real-time integrated approaches to ore characterisation. Integrating HSI, automated mineralogy, and portable X-ray fluorescence (pXRF) helps with inclusive geochemical analysis and improved understanding of the ore mineralogical characteristics.

## 2. Geolology of the bushveld igneous complex

The 2.055 Ga BIC is the world's largest and most studied mafic–ultramafic layered intrusion (Naldrett et al., 2012; Gleason et al., 2011; Maier et al. 2013; Zeh et al. 2015; Mungall et al. 2016; Scoates et al. 2021, Hayes et al., 2024). The BIC consists of eastern, western and northern limbs (Fig. 1). It spans an area of 66,000 $km^2$ and has an average thickness of ~8 km (Maier et al., 2013; Zeh et al., 2015; Mayer et al., 2021). The large-scale layering within the BIC allows for a distinct subdivision of geological layers, as shown in Fig. 1. Notably, the layers are largely laterally continuous, with only minor downward magmatic erosional discontinuities, referred to as potholes (Pebane and Latypov, 2017). This lateral continuity is beneficial for exploration, evaluation of economic sequences, mine planning, and operations. The upper Critical Zone of the BIC contains the world's largest concentration of PGEs (Barnes et al., 2004; Mudd et a., 2018). Mineralisation occurs in three main reefs, namely: **(i)** the Upper Group Chromitite No. 2 (UG-2), **(ii)** Merensky Reef and **(iii)** Platreef.

The Merensky Reef is characterised by significant variations in thickness, composition, and mineralisation positioning (Smith et al., 2021). The rock-forming minerals in the Merensky Reef consist of nearly equal proportions of dark iron-magnesium silicates and lighter calcium-aluminium-sodium silicates, with 5 to 15 mm chromite layers above and below the Reef (Schouwstra et al., 2000; Smith, 2011; Amponsah-Dacosta, 2017). The total thickness of Merensky Reef package ranges from 10 to 30 cm (Boudreau, 2008; Chistyakova et al., 2019). The Merensky Pegmatoid, contains most of BMS and associated PGEs (Wirth et al., 2013; Price, 2016). The Merensky Reef extends for 300 km along the outcrops of the eastern and western limbs of the BIC and reaches depths of up to 5 km (Mayer et al., 2021).

The silicate minerals in the Merensky Reef are predominantly orthopyroxene (~60 %), plagioclase feldspar (~20 %), pyroxene (~15 %), phlogopite (5 %), and occasional olivine (Gibson et al., 2023). Secondary minerals, such as talc, serpentine, chlorite, and magnetite, are widespread across the BIC (Becker et al., 2009). The BMS include pyrrhotite (~40 %), pentlandite (~30 %), chalcopyrite (~15 %), along with trace amounts of millerite (NiS), troilite (FeS), pyrite ($FeS_2$), and cubanite ($Cu_5FeS_4$) (Godel et al., 2007). The primary platinum group minerals (PGMs) are cooperite (PtS), braggite [(Pt, Pd)NiS], sperrylite ($PtAs_2$), and PGE alloys, with laurite ($RuS_2$) being abundant in some areas (Prichard et al., 2004; Osbahr et al., 2013; O'Connor and Alexandrova, 2021).

### 2.1. Mineralisation mechanism

Layered intrusion provinces such as the BIC (South Africa), Dufek (Antarctica), Duluth (USA), Stillwater (USA), Muskox (Canada), Great Dyke (Zimbabwe), Kiglapait (Canada), Skaergaard (Greenland), Panzhihua (China), and Rum (Scotland) comprise igneous rocks that cooled slowly (Latypov et al., 2024). Silicate minerals crystallise and accumulate to form igneous rocks. As the magma cools, its mineral composition changes progressively due to a slow decrease in temperature. Early crystallising silicate minerals are rich in magnesium and iron, associated with mafic magma, form at higher temperatures. In contrast, calcium, aluminium, and sodium-rich silicates crystallise at lower temperatures, corresponding to the silicic facies. This systematic change in mineral composition is termed magma fractionation.

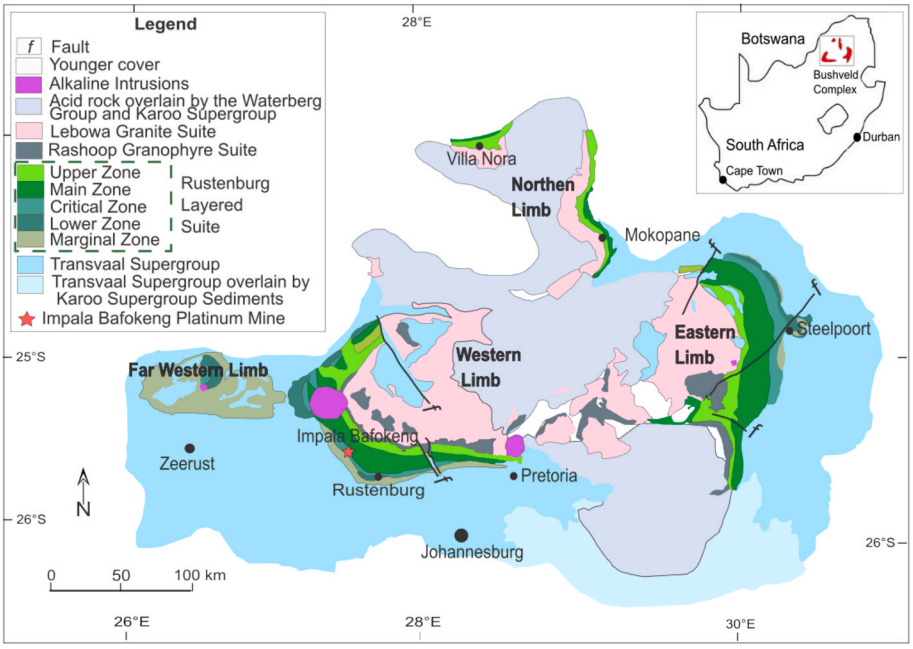


**Fig. 1.** A simplified map of the Bushveld Complex, showing its three major limbs, key towns, and the location of the Impala Bafokeng Platinum Mine (IBPM). The map is modified after Chistyakova et al., 2021.

The surplus magma enters (or intrudes) the chamber and undergoes cooling, this process repeats multiple times until several kilometres of solid rock accumulate (Naldrett et al., 2009, 2012; Cawthorn, 2015, Latypov et al., 2017). The layering formed during this process exerts significant control over the distribution of ore deposits (McDonald and Holwell, 2011). Minerals such as chromite ($Cr_2O_3$), ilmenite ((Fe, Mn, Mg)$TiO_3$), and PGMs are typically associated with mafic layers, whereas magnetite ($Fe_3O_4$), cassiterite ($SnO_2$), and zircon are more common in silicic layers (Kinnaird, 2005).

Large layered igneous provinces ore forming processes are generally attributed to the gravitational settling of specific minerals, the influx of compositionally distinct magma, magma-rock interaction, or immiscibility of a melt. Minor variations in magma composition can lead to the formation of chromite-rich layers during these processes, resulting in the rock type known as chromitite, which is commonly found in layered intrusions. Occasionally, changes in magma composition produce layers rich in iron, nickel, and copper sulphides, along with arsenides, tellurides, and alloys of PGEs, leading to the formation of platinum group mineral (PGM) bearing ores.

## 3. Material and methods

A total of six drill core trays of Merensky Reef were obtained from the IBPM, situated on the western limb of the BIC near Rustenburg, South Africa (Fig. 1). The trays have a length of 1.5 m and width of 0.4 m. The drill cores were subjected to a multi-stage analytical workflow integrating HSI, pXRF, automated mineralogy, and conventional laboratory-based techniques (i.e., XRD) to ensure a complete mineralogical and

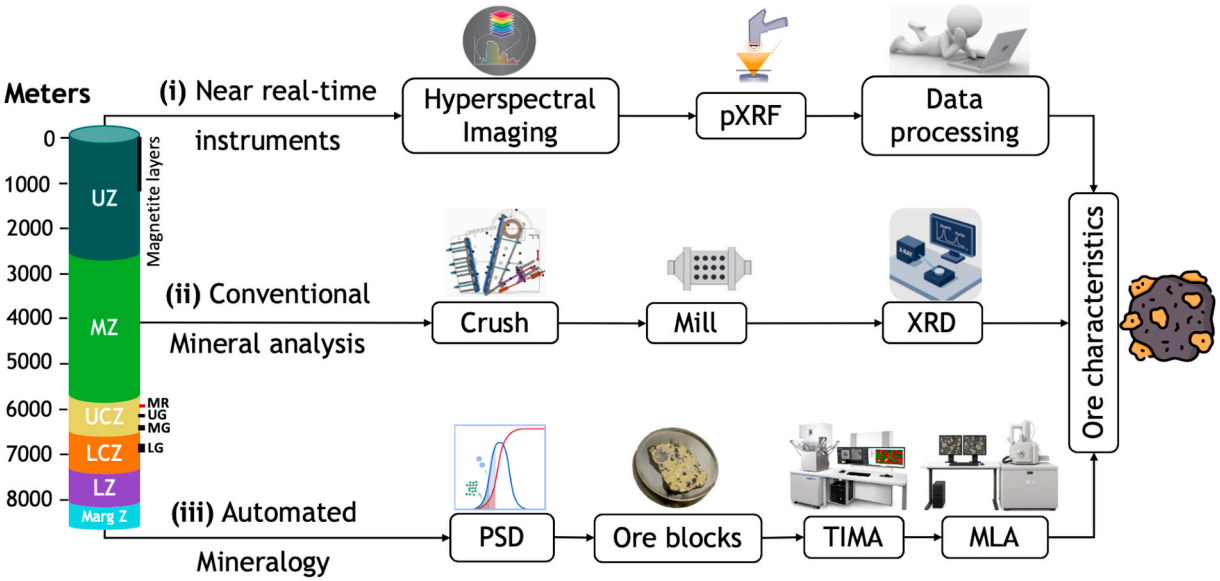


**Fig. 2.** A schematic methodology workflow for ore characterisation using near real-time, conventional and automated mineralogy analysis. UZ = upper zone, MZ = Main Zone, UCZ Upper critical zone, LCZ = Lower critical zone, LZ = Lower Zone and Marg. Z = Marginal Zone.

geochemical characterisation (Fig. 2).

### 3.1. Hyperspectral imaging (HSI)

A near real-time HSI was used as the initial step of the Merensky Reef ore analytical workflow (Fig. 2). Spectral data were acquired using the SisuROCK HSI Scanner, housed at the Council for Geoscience, Pretoria. The scanner is fitted with three cameras covering the visible–near infrared (VNIR: 380–1,000 nm), short-wave infrared (SWIR: 1,000–2,500 nm), and long-wave infrared (LWIR: 7,700–12,300 nm) ranges. An RGB camera for high-resolution natural colour imaging is also integrated into the HSI. The VNIR–SWIR range was captured by the FENIX sensor, while the OWL camera was used for LWIR acquisition. Spatial resolution was ±1.4 mm (hyperspectral) and ±0.12 mm (RGB), with a scan rate of 170 mm/s. Spectral calibration is conducted daily using standard reference materials (i.e., filter glass, polystyrene, and polypropylene) to monitor wavelength stability and ensure spectral accuracy within one band spacing for each sensor range. Known rock samples (e.g., quartz, carbonate) were also scanned to verify camera performance.

The HSI data were processed using TerraCore's Intellicore® system, in a five-steps workflow. (**i**) corrected sensor radiance to reflectance using reference panels, applied geometric correction, and cropped the images; (**ii**) generated a mask to isolate the drill core from background materials, enabling rapid generation of first-pass mineral maps to support real-time core logging; (**iii**) applied advanced spectral processing routines, extracting absorption features and mineral indicators across VNIR–SWIR (e.g., depth, width, wavelength) and LWIR (e.g., peak position, height). Automated mineral maps were generated using Pearson correlation against spectral libraries and unsupervised clustering via Self-Organising Maps (SOMs); (**iv**) expert spectral interpretation and refinement of dominant mineral classifications using the USGS VNIR–SWIR and Johns Hopkins LWIR spectral libraries. Misclassified or mixed spectra were manually reclassified based on their dominant and subordinate features. (**v**) compiled all processed outputs into standardised products accessible via Intellicore® for further interpretation by project geologists.

The VNIR–SWIR data is effective for mapping hydrated silicates (e.g., clays, micas, gypsum), while LWIR data allows for the identification of anhydrous silicates and carbonates (e.g., quartz, feldspar, calcite, pyroxene). Collectively, the high-resolution spectral maps provide rapid mineralogical discernments across the entire drill core. This allows the delineation of lithological boundaries and alteration zones for subsequent sampling and validation.

### 3.2. Portable X-ray fluorescence (pXRF)

Complementing the HSI mineralogical analysis, real-time pXRF scanning was conducted on the same drill core at the University of the Witwatersrand. pXRF is a handheld, non-destructive analytical instrument capable of providing rapid, in-situ, multi-elemental analysis without laboratory preparation. The pXRF instrument was positioned directly on the core surface to scan at 30 cm intervals. Primary X-rays excited atoms within the sample, inducing the emission of secondary (fluorescent) X-rays characteristic of the constituent elements. The resulting geochemical data was immediately available to the operator for real-time interpretation.

The pXRF data provided elemental distribution profiles, important for identifying geochemically anomalous zones enriched in base metals and other elements. This geochemical data was used in conjunction with HSI-derived mineralogical maps to improve the spatial interpretation of lithological, mineralogical, and alteration patterns along the core. The integration of both datasets enabled early identification and preselection of zones of potential PGE high grades. This approach guided subsequent high-precision laboratory analyses by targeting intervals showing spectral (mineralogical or lithological) and elemental anomalies.

### 3.3. X-ray diffraction (XRD)

A total of four subsamples, selected from distinct drill core intervals representing anorthosite and norite lithologies, were analysed using XRD. The subsamples labelled A, B, C and D correspond to depth intervals of 10.7–10.8 m, 10.0–10.1 m, 3.6–4.1 m, and 1.3–1.4 m, respectively. Subsample A and B are representative for anorthosite while C and D are representative subsamples for norite. XRD analysis was conducted at the XRD Analytical & Consulting Laboratory in Pretoria, South Africa. Each subsample was pulverised and prepared using the back-loading method to attain random particle orientation. Diffractograms were acquired using a Malvern Panalytical Aeris diffractometer equipped with a pixel detector, fixed slits, and Fe-filtered Co-Kα radiation. Mineral phase identification and quantification were performed using X'Pert High-Score Plus software. Minor peaks that could not be matched suggest the presence of trace mineral phases. Phases occurring below 0.5 wt% were considered unreliable, and amorphous phases, if present, were not quantified.

### 3.4. Normative mineralogy

To improve interpretability, normative mineralogy calculations (CIPW norm) modified by Verma et al. (2003) after Cross et al. (1902), were applied to transform the pXRF geochemical dataset into estimate mineral phase proportions. This approach assumes that the ore has not undergone any hydrothermal alteration, providing a basic magmatic mineralogy. This allows for validation of the accuracy and representativity of HSI and pXRF in capturing mineralogical variability.

### 3.5. Laboratory based PGEs and base metals assays

A total of six subsamples were assayed for 4E PGE grades using Inductively Coupled Plasma Optical Emission Spectroscopy (ICP-OES) at Suntech Geomet Laboratory in Johannesburg. Samples A–D correspond to those previously analysed using XRD (Section 3.3), while E and F were collected from depths of 4.65–4.85 m and 8.45–9.05 m, representing norite and anorthosite lithologies, respectively. Each sample was pulverised to 80 % passing 75 μm, mixed with a lead-based flux and silver nitrate co-collector, and fused at 1050 °C to produce a PGE-rich button and slag (discarded). The button was cupellated at 950 °C using porous cupels to yield a prill, which was digested in aqua regia, diluted with deionised water, and analysed by ICP-OES.

Detailed X-ray fluorescence (XRF) analysis, including base metal quantification, was also performed on all six subsamples. These analyses aimed at showing correlations between base BMS and PGE grades, supporting the hypothesis that BMS distributions can serve as proxies for identifying PGE-enriched zones. The results will also be used to evaluate the effectiveness of pXRF as a rapid tool for delineating PGE mineralisation.

### 3.6. Comminution and particle size distribution

Comminution tests on the remainder of the drill core were conducted at the University of the Witwatersrand. Primary crushing was performed at the school of geosciences using a jaw crusher to produce coarse rock fragments ranging from 20 to 35 mm. The crushed material was subsequently subjected to secondary crushing using a cone crusher at the school of chemical and metallurgical engineering, reducing the particle sizes to ~5 mm. The bulk sample was homogenised, and representative 1 kg subsamples were obtained using a rotary sample splitter to ensure uniformity. Each subsample was sieved to remove particles larger than 5 mm prior to milling. Wet grinding was carried out using a rod mill with chrome steel rods (length = 500 mm, diameter = 25 mm) at a pulp solid concentration of ~30 % (w/v). The mill had an internal diameter of 200

mm and a length of 600 mm and was operated at 75 rpm, corresponding to 75 % of the maximum speed. Milling durations ranged from 0 to 50 min to evaluate time-dependent grinding behavior. Subsequent to each milling interval, the pulp was discharged, wet sieved and dried at 60 °C. Particle size distribution was determined using wet sieving in accordance with ASTM C136/C136M-14 standards. The sieving sequence ranged from 212 μm to 10 μm, with particular focus on the 75 μm screen. Grinding performance was quantified using the $P_{80}$ value (i.e., 80 % of the material passes 75 μm), which served as the primary metric for comminution efficiency.

### 3.7. Automated mineralogy

The final phase of the workflow involved detailed ore characterisation using automated mineralogy. Specifically, the TESCAN TIMA and MLA analyses were conducted at the University of the Witwatersrand and Mintek. For these analyses, the drill core was crushed, milled, screened to acquire PSD, and homogenised to get representative samples as detailed in section 3.5. Automated mineralogy combines scanning electron microscopy (SEM) with energy-dispersive X-ray spectroscopy (EDS) to provide high-resolution quantitative mineralogical data. TESCAN TIMA was mainly used to acquire bulk mineralogy, mineral liberation characteristics and mineral associations. MLA was specifically used for PGE phase identification and their associations with sulphides or gangue as well as cross validating the TIMA results. The automated mineralogy results are important in defining mineral deportment trends, particularly PGEs. The results also serve as a benchmark to evaluate the accuracy or limitations of HSI and pXRF, allowing for an integrated comparison between rapid scanning techniques and detailed, laboratory-based analyses.

### 3.8. Comparative valuation

A comparative evaluation was conducted to assess the correlation between the near real-time methods (HSI and pXRF) and traditional laboratory techniques (XRD and automated mineralogy). This integrated valuation helps in determining the reliability of using rapid, non-destructive techniques for mineralogical and geochemical characterisation, particularly in the context of drill core analysis and PGE ore evaluation.

## 4. Results

### 4.1. Near real-time (HSI and pXRF) and XRD analysis

HSI allows for rapid and non-destructive mineral identification based on spectral features, making it an efficient tool for large-scale analysis. pXRF complements HSI by providing detailed geochemical data, essential for quantifying elemental compositions. XRD, in turn, confirms available mineral phases, enhancing the reliability of mineralogical interpretations.

The mineralogical results offer a general perspective on the ore's geometallurgical characteristics. The lithology of the drill core consists of norite and anorthosite (Fig. 3a). The HSI results show that mineral composition of the low-grade Merensky Reef ore is predominantly composed of pyroxene (more orthopyroxene than clinopyroxene), plagioclase (anorthite), olivine, and minor traces of quartz. Secondary or alteration minerals include serpentine, prehnite, amphibole, talc, chlorite and traces of epidote (Fig. 3b). Specifically, Samples A and B showed high plagioclase contents, consistent with the mineralogical signature of anorthosite rocks. Conversely, Samples C and D have mineralogical characteristics pointing towards norite (Fig. 3c). The normative mineralogy derived from pXRF-based geochemical conversions aligns with mineralogical data from both HSI and XRD analyses (Fig. 3c). These results showcase the capability of these techniques to delineate different minerals and rock types accurately, which can be importance in mineral exploration and for selective mining.

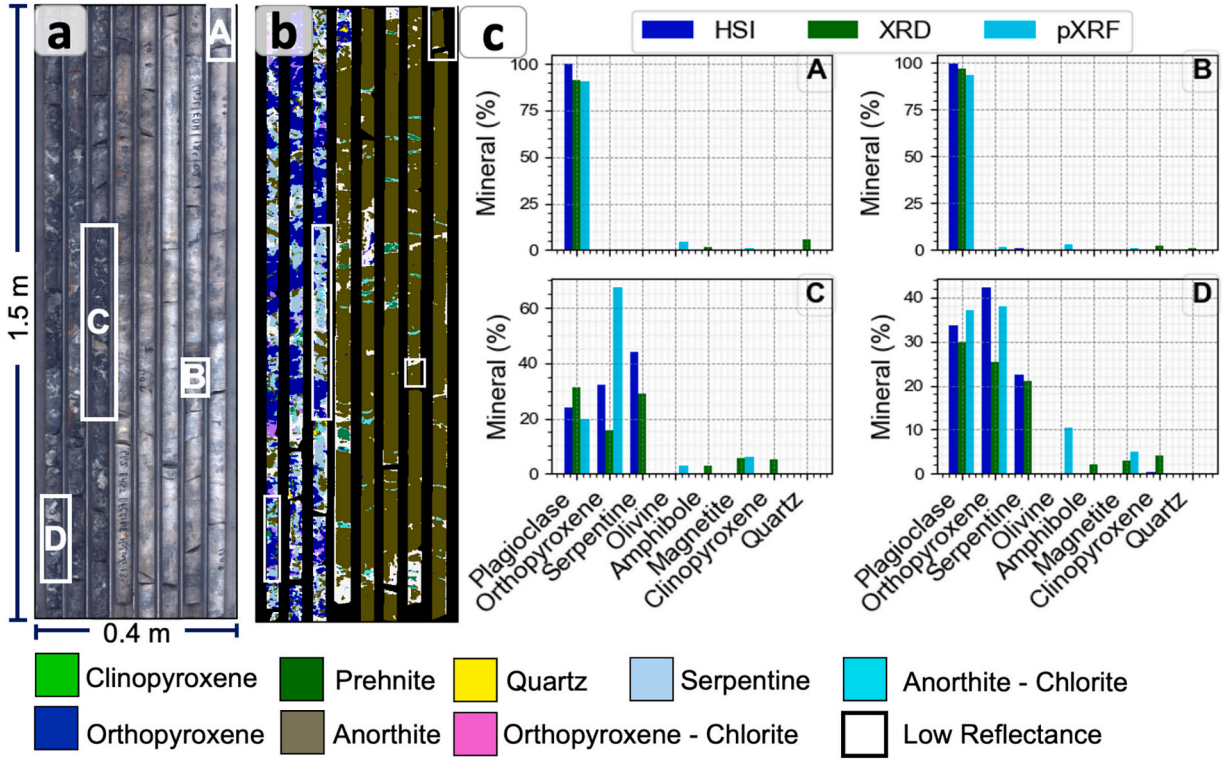


**Fig. 3.** HSI results (a, b) with sampled sections (A, B, C and D) and comparative mineralogical analysis using HSI, XRD, and pXRF-derived Normative Mineralogy in c. a. shows RBG image; b. shows HSI mineral phases determined using Long-Wave Infrared (LWIR) spectrum and c. compares mineral compositions from HSI, XRD and pXRF Normative mineralogy.

### 4.2. pXRF Assays: Proxy for PGE grades?

The pXRF geochemical data shows a strong correlation between sulfur (S), Ni, Cu, and Co, with higher grades observed in noritic rocks compared to anorthitic lithologies. This geochemical trend indicates the presence of BMS minerals such as pyrrhotite ($Fe_{1-x}S$), pentlandite ($(Fe, Ni)_9S_8$), chalcopyrite ($CuFeS_2$), and cobaltite (CoAsS) at economically concentrations in the ore. The enrichment of these elements in noritic rocks aligns with well-documented sulphide mineralisation processes, where S plays important role in metal transport and deposition (Naldrett, 2013).

The co-occurrence of Ni, Cu, and Co within sulphide phases accentuates their geochemical affinity with S, which is essential for understanding both the genesis of mineralisation and the economic viability of the ore deposit. The observed element associations suggest that the sulphide minerals formed under conditions favourable for metal enrichment, likely through magmatic segregation or hydrothermal remobilisation. The association between BMS and PGEs is well-established in BIC (Rose, 2016). Therefore, vertical log concentration patterns of S, Ni, Cu, and Co acquired using pXRF analyses can serve as proxies to identifying or predicting zones of high-grade PGE mineralisation within the core (Fig. 4).

### 4.3. Statistical analysis of BMS

The elemental distribution of BMS (Ni, Cu, Co, and Zn) in the analysed drill core provides important discernments into potential PGEs enrichment zones, particularly in magmatic sulphide systems. Nickel has variable grades, with a mean of 0.28 %, a median of 0.17 %, and a standard deviation of 0.55 % (Fig. 5). The highest pXRF recorded Ni grade is 2.68 %, suggesting localized sulphide enrichment. Ni is a key indicator of sulphide mineral saturation; the high-grade values of Ni may correspond to sections of the core where PGE-bearing sulphide phases have accumulated. Cu shows a mean grade of 0.06 %, a median of 0.01 %, and a standard deviation of 0.18 %. Although Cu grades are relatively low, the highest recorded value of 1.21 % suggests the presence of localized Cu-rich sulphides such as chalcopyrite, which are known to host PGEs through solid solution or micro-inclusions.

Cobalt is often associated with pentlandite and other sulphides, has a mean grade of 0.05 %, a median of 0.04 %, and a standard deviation of 0.03 % (Fig. 5). The highest detected grade value is 0.15 %, reinforcing the presence of Ni-Co sulphide phases that may serve as carriers for PGEs. Given that Co often coexists with PGE-hosting minerals in sulphide ores, these grades indicate zones where PGE enrichment could be expected. Zinc has relatively low grades, with a mean of 0.04 %, a median of 0.03 %, and a standard deviation of 0.03 % (Fig. 5). The maximum recorded grade of 0.18 % may be indicative of minor sphalerite occurrences. Zn is not a direct indicator of PGE mineralization. However, the presence of Zn in sulphide zones may reflect fluid interaction processes that could influence PGE redistribution. The observed distributions of BMS elements suggest that certain sections of the core may host PGE mineralization. These results have been further investigated using automated mineralogy (i.e., TIMA) to confirm the presence of PGEs and assess their deportment within the sulphide phases.

### 4.4. Correlation of PGEs and base metals

The assay results show distinct geochemical trends in the distribution

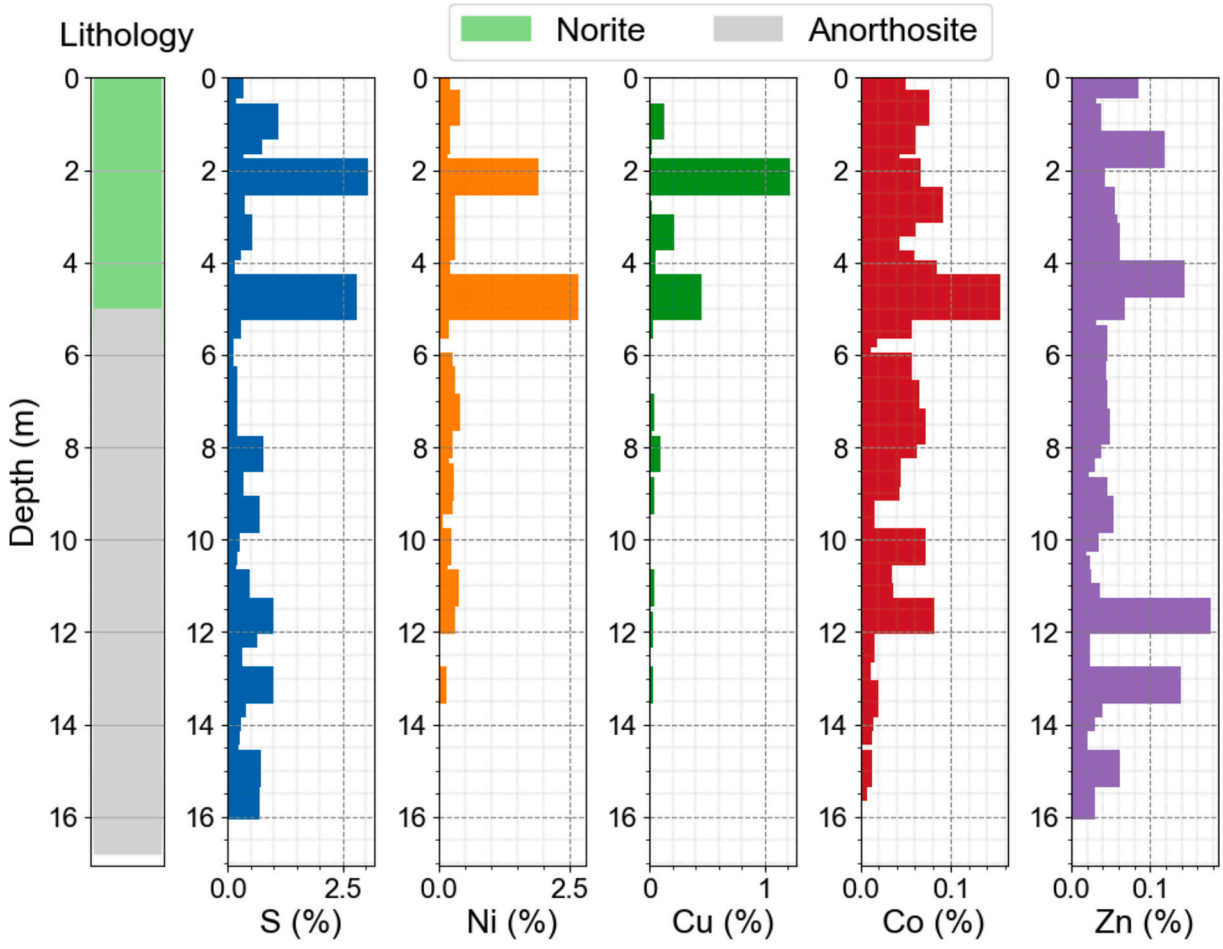


**Fig. 4.** Lithological log and vertical BMS elemental distributions as determined by pXRF.

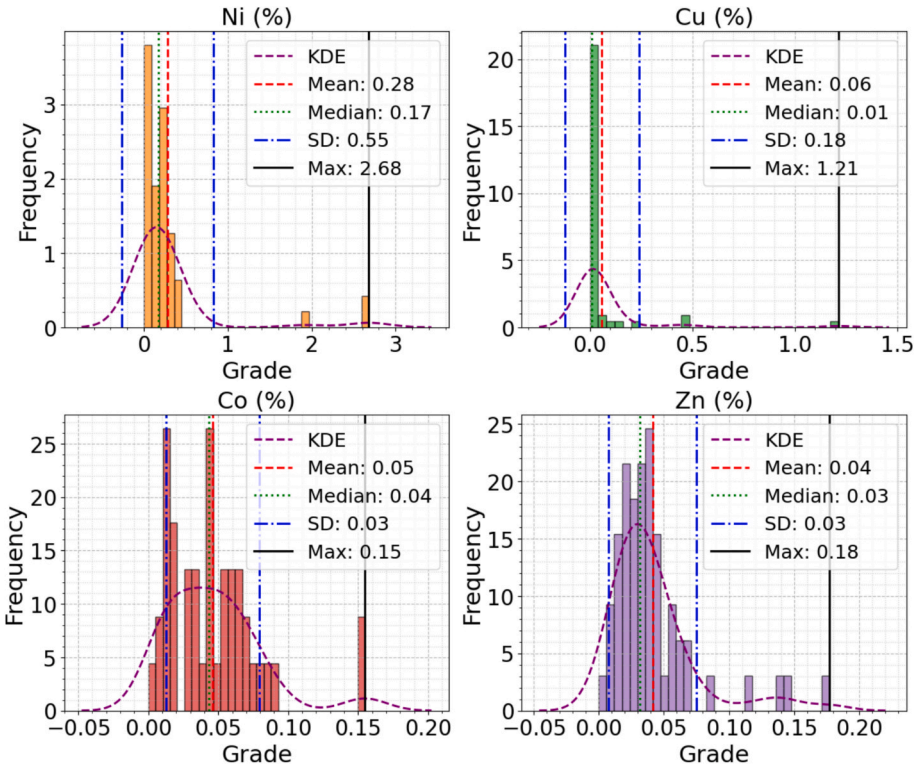


**Fig. 5.** Histograms illustrating the statistical grade distribution of BMS within the analysed core. KDE = Kernel Density Estimation.

of PGEs (Pt, Pd, Rh), gold (Au), and associated base metals (Ni, Cu, Co) across lithological units. The drill core mainly consists of anorthosite and norite. A total of six subsamples (A to F) were analysed, with three samples coming from each lithology.

The distribution of PGEs and Au across the analysed drill core subsamples shows a strong association with base metals (Ni, Cu, and Co) and is notably influenced by lithology (Table 1). A distinct contrast in elemental concentrations is observed between anorthosite and norite units. Samples hosted in norite (C to E) have higher concentrations of PGEs and Au, with Pt ranging from 0.31 to 3.59 g/t, Pd from 0.46 to 7.10 g/t, Rh up to 0.75 g/t, and Au reaching a maximum of 3.12 g/t. In contrast, anorthosite-hosted samples (A, B and F) show considerably lower values, with Pt below 0.3 g/t, Pd $\leq$ 0.34 g/t, and Au not exceeding 0.91 g/t. Rh was below detection (<0.01 g/t) in two of the three anorthosite samples.

The base metal content mirrors this trend. Norite samples show high grades of Ni (up to 4.85 %), Cu (up to 3.57 %), and Co (up to 0.374 %), resulting in a cumulative (Ni + Cu + Co) content as high as 8.79 %. In contrast, anorthosite samples have a maximum cumulative base metal grade of only 0.48 %. This suggests a strong lithological control on metal endowment, with norite being the primary host of both PGEs and associated base metals.

Pearson correlation analysis indicates positive relationships between PGEs/Au and base metals (Fig. 6), particularly in Noritic samples. For instance, Pt and Pd show strong correlation with Ni and Cu, suggesting co-occurrence possibly due to sulphide mineral associations. Rh and Au also have positive correlation with Ni and Cu, although the relationship appears less pronounced in low-grade anorthosite samples. These observations imply that base metal sulphides can serve as proxies for PGE mineralisation in norite, providing a valuable vectoring tool for exploration and metallurgical targeting.

### 4.5. *Particle size distribution (PSD)*

The PSD curves for sample A and sample B were determined through sieve analysis, and the cumulative passing percentages were plotted against grain size (μm) on a semi-logarithmic scale (Fig. 7). The results demonstrate distinct variations in PSD between the two samples. Sample A displays a coarser particle distribution, with 67.5 % passing 75 μm and 36.1 % passing 38 μm. In contrast, sample B is finer, with 84.2 % passing 75 μm and 39.3 % passing 38 μm. The fine nature of sample B is further evident at middle size fractions with 57.9 % of the ore material passing 53 μm, compared to 46.6 % in sample A. The average PSD from the two samples has 76 % of the material passing 75 μm. The high proportion of fine particles in sample B indicates differences in milling efficiency between the two samples. The fine grain size fraction in sample B suggests high mineral liberation than the coarser fraction in sample A. This could potentially influence downstream processing performance. Interpolation using the Piecewise Cubic Hermite Interpolating Polynomial provides a smooth of true PSD data points. The semi-logarithmic plot shows

**Table 1**
4E PGE (g/t) and base metal (%) assays as determined by ICP-OES and XRF, respectively.

| ID | Depth. From-To (m) | Pt | Pd | Rh | Au | Ni | Co | Cu | Lithologies |
|---|---|---|---|---|---|---|---|---|---|
| A | 10.7–10.8 | 0.19 | 0.04 | <0.01 | 0.91 | 0.141 | 0.021 | 0.107 | Anorthosite |
| B | 10.0–10.1 | 0.21 | 0.31 | 0.05 | 0.13 | 0.234 | 0.028 | 0.189 | Anorthosite |
| C | 3.6–4.1 | 0.31 | 0.46 | 0.04 | 0.04 | 0.165 | 0.092 | 0.292 | Norite |
| D | 1.3–1.4 | 2.51 | 3.45 | 0.45 | 0.18 | 0.285 | 0.087 | 0.975 | Norite |
| E | 4.65–4.85 | 3.59 | 7.10 | 0.75 | 3.12 | 4.852 | 0.374 | 3.568 | Norite |
| F | 8.45–9.05 | 0.26 | 0.34 | <0.01 | 0.06 | 0.083 | 0.054 | 0.339 | Anorthosite |

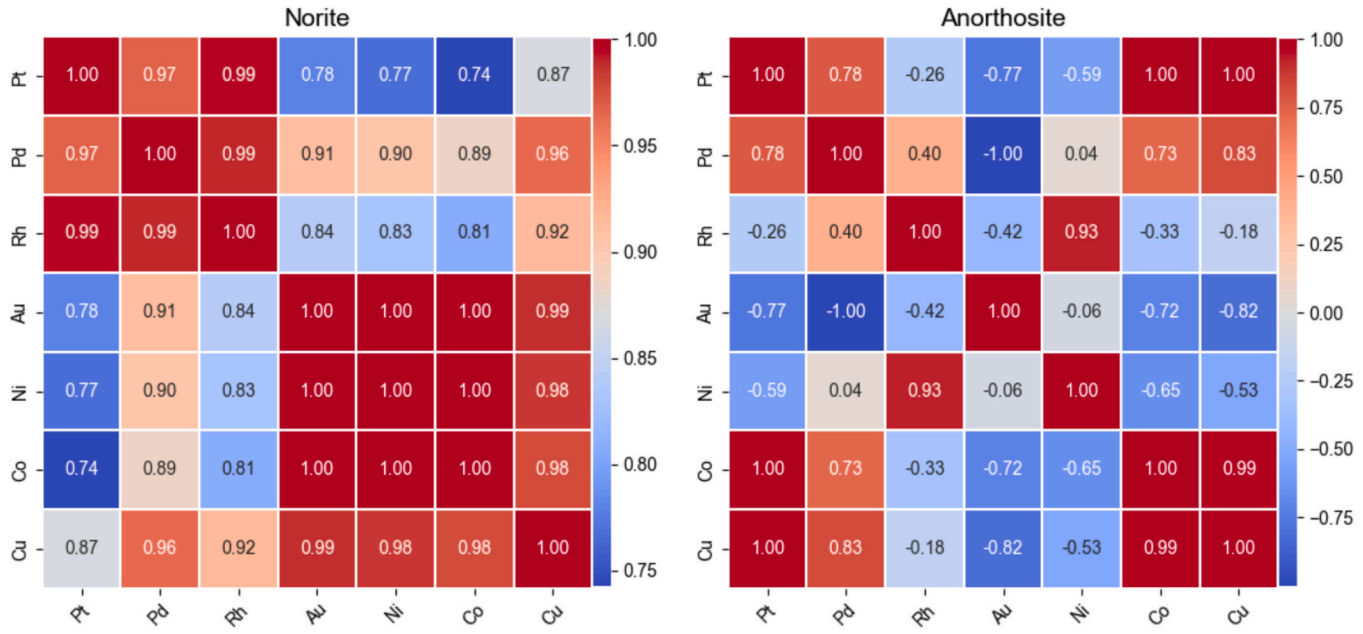


**Fig. 6.** Heatmaps showing correlation of PGEs and base metals.

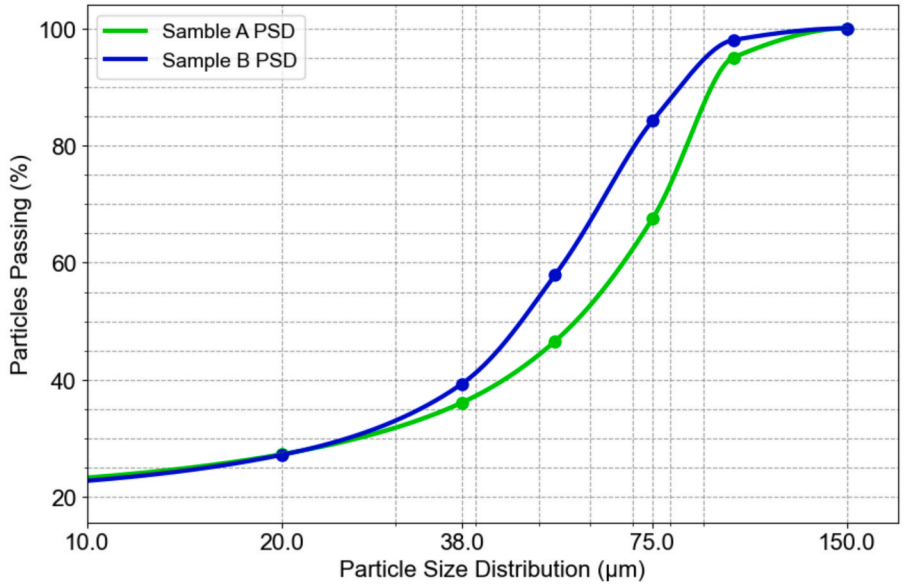


**Fig. 7.** Particle Size Distribution of ore samples (A and B) showing proportions of particles passing through different screen sizes.

a typical sigmoidal distribution grinding trend. These results are important for optimizing comminution and subsequent beneficiation processes.

The representative subsamples from both ore materials (sample A and B) of each size fraction were used to prepare polished ore blocks. The ore blocks were analysed using TIMA and MLA to determine ore mineralogical characteristics. Different size fractions were processed separately to improve analytical accuracy before being re-combined into a single dataset, weighted according to their respective masses. This approach strengthens the correlation between PSD and mineral liberation characteristics.

### 4.6. Automated mineralogy

TIMA analysis was conducted to determine bulk ore mineralogy, generate mineral and elemental maps, and evaluate mineral associations, ore liberation characteristics and PGE deportment. Mineral-chemistry reconciliation was performed in conjunction with XRF geochemistry to validate bulk mineralogy.

#### 4.6.1. TESCAN integrated mineral Analyzer (TIMA) analysis

The bulk mineralogy of the analysed samples predominantly consists of silicate minerals, with pyroxene (61.98 wt%), feldspar (25.36 wt%) and amphibole (1.09 wt%) being the most abundant phase (Fig. 8a). This mineralogical composition indicates a primary magmatic origin (mafic to ultramafic rock assemblages), which is consistent with Merensky Reef. The presence of olivine (0.75 wt%), serpentine (3.00 wt%), and chlorite (0.91 wt%) indicates varying degrees of hydrothermal alteration and metamorphic processes. This is further supported by the presence of talc (0.71 wt%) and mica (0.39 wt%) which are related to

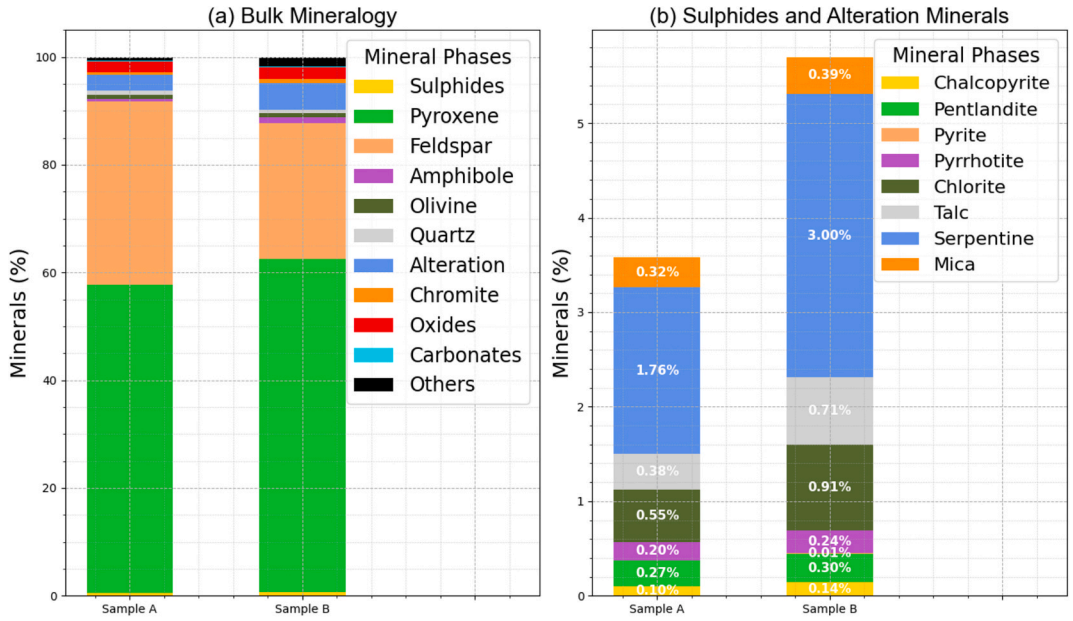


**Fig. 8.** Stacked graphs showing. (a) Bulk mineralogy and (b) Sulphide and alteration group minerals as determined by TIMA.

serpentinisation and hydration reactions.

The TIMA microphotographs (Fig. 9) present visually support for the bulk mineralogical composition and elemental distribution of base metals within the sample. Microphotograph (a) illustrates the predominance of silicate minerals, corroborating the bulk mineralogical data (Fig. 8a), which identifies pyroxene and feldspar as the principal phases. Elemental distribution maps in microphotographs (b), (c), and (d) show the spatial presence of base metals (i.e., Cu, Fe, and Ni) in the mineral matrix. Notably, microphotograph (d) confirms the occurrence of Ni in association with pentlandite, in concord with the sulphide mineral phases identified in bulk analysis (Fig. 8b), where pentlandite was the dominant sulphide mineral.

The mineralogical association data provides important information about distribution or interactions of BMS and gangue minerals. The results shows that chalcopyrite, pentlandite, and pyrrhotite have high free surface (i.e., degree of liberation) proportions of 72.38 %, 75.09 %, and 62.81 %, respectively (Fig. 10). The grouped BMS category shows a similar trend, with 75.45 % classified as free surface, implying that the sulphide minerals are largely exposed, potentially augmenting their floatability. Chromite demonstrates a significant free surface proportion

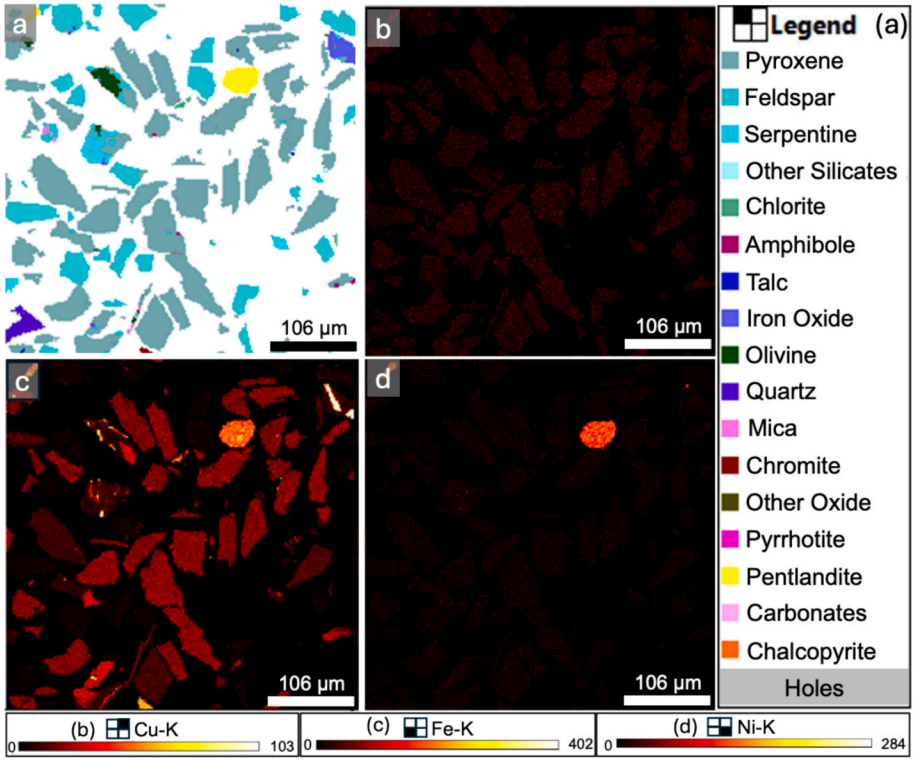


**Fig. 9.** TIMA microphotographs showing bulk mineralogy and base metal elemental maps.

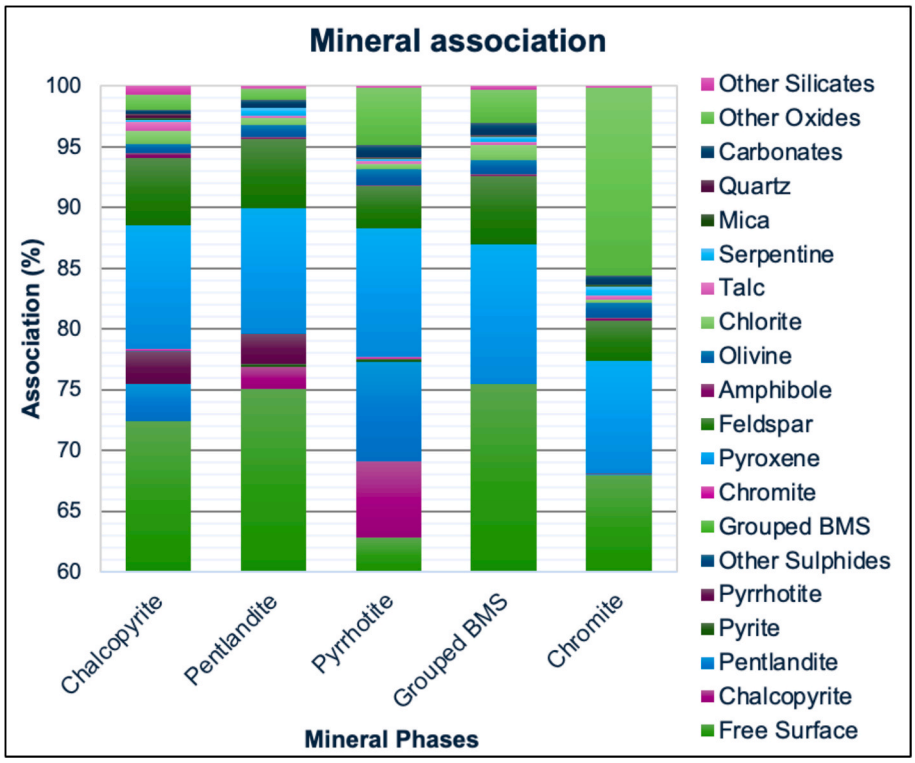


**Fig. 10.** A stacked graph showing the mineralogical associations, specifically shows the relationship between BMS and gangue minerals, as determined by TIMA.

(67.96 %), indicating its discrete occurrence in the ore matrix. The mineral interlocking characteristics shows notable associations between sulphides. Pyrrhotite demonstrates notable associations with pentlandite (8.18 %) and chalcopyrite (6.29 %). This indicates that a portion of pyrrhotite is locked within these sulphide mineral phases. Similarly, pentlandite shows an appreciable association with chalcopyrite (3.06 %), indicating the interconnected nature of the BMS phases. The occurrence of pyrite is relatively minor, with low associations across all sulphide minerals.

Gangue minerals, mainly pyroxene, feldspar, and other silicates, are strongly associated with BMS phases (Fig. 10). Pyroxene has relatively uniform association distribution across chalcopyrite (10.21 %), pentlandite (10.34 %), pyrrhotite (10.60 %) and the grouped BMS category (11.46 %). This shows that pyroxene is a major gangue mineral associated with BMS. Feldspar associations with chalcopyrite (5.55 %) and pentlandite (5.72 %) are low. This indicates that chalcopyrite and pentlandite may be encapsulated within silicate matrices. The presence of chlorite, amphibole, and serpentine is relatively minor, with very low to immensurable associations. The “other oxides” (e.g., rutile, ilmenite, hematite, and goethite) have lower but significant associations with pyrrhotite (4.69 %) and grouped BMS (2.76 %), suggesting potential oxidation of sulphides or iron-rich mineral alteration. Chromite, a significant component in BIC ore types, shows low but measurable associations with BMS phases, specifically, pyrrhotite (0.10 %) and grouped BMS (0.06 %), indicating potential challenges in its selective rejection during flotation.

### 4.6.2. *Liberation characteristics*

Cumulative liberation by surface exposure (i.e., free surface) reveals measurable differences in the exposure of base metal sulphides (BMS) and chromite between the two samples (ore types). Pentlandite shows a high degree of liberation in Sample A, with 87.1 % of particles achieving

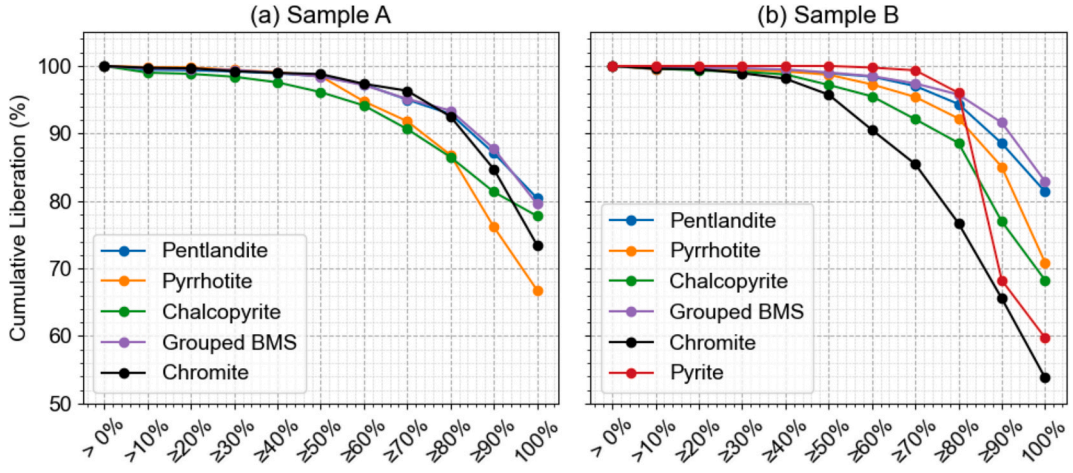


**Fig. 11.** Cumulative liberation curves by surface exposure for base metal sulphides and chromite in Sample A and Sample B.

≥ 90 % surface exposure and 80.4 % fully liberated (Fig. 11a). Pyrrhotite follows with 76.2 % ≥90 % liberation and 66.8 % at 100 % exposure, while chalcopyrite has 81.4 % and 77.8 %, respectively. The grouped BMS collectively show 87.8 % of particles ≥ 90 % liberated and 79.6 % fully liberated.

Improved sulphide liberation is observed in Sample B (Fig. 11b). Pentlandite achieves 88.6 % liberation at the ≥90 % surface exposure and 81.4 % at full liberation. Pyrrhotite and chalcopyrite report 85.1 % and 77.0 % of particles ≥90 % liberated, with 70.9 % and 68.3 % reaching full liberation, respectively. Grouped BMS show the highest overall liberation in Sample B, with 91.6 % at ≥90 % surface exposure and 82.9 % fully liberated. Pyrite, absent from Sample A, is also well liberated in Sample B, with 68.3 % of particles ≥90 % exposed and 59.8 % fully liberated. A contrasting trend is observed for chromite. Liberation is higher in Sample A, with 84.7 % of particles reaching ≥90 % liberation and 73.5 % fully liberated, compared to 65.6 % and 53.8 % in Sample B, respectively. These differences in liberation behavior are attributable to variations in mineral texture, grain size, or intergrowths.

#### 4.6.3. *Mineral liberation Analyser (MLA)*

The mineralogical analysis using MLA confirms that BMS are predominantly associated with pyroxene, particularly enstatite (Fig. 12). Among the BMS, pyrrhotite has the strongest association with enstatite, followed by pentlandite and chalcopyrite. The gangue mineralogy includes plagioclase, magnetite, hornblende, mica, and chlorite, with limited association with BMS. MLA further confirms that enstatite and plagioclase are the primary gangue minerals associated with both BMS and PGEs (Fig. 12a).

A total of 60 PGE grains were identified from 30 ore blocks. Of these, 16 grains (21.2 %) were fully liberated, while 12 grains (49.3 %) were associated with liberated BMS, primarily pyrrhotite (Fig. 12A). Three grains (0.8 %) were associated with BMS locked within silicate or oxide gangue, and five grains (19.3 %) were attached directly to silicate or oxide gangue. A further 15 grains (7.7 %) were associated with BMS that were themselves attached to gangue phases, and 9 grains (1.6 %) were completely locked within silicate or oxide gangue matrices (Fig. 12c). Among the 16 liberated grains, 9 (56.3 %) shown an equivalent circular diameter of less than 3 μm. This fine grain size suggests that although these grains are technically liberated, their recoverability via conventional flotation processes may be limited due to their small size and high surface area to volume ratio.

The dominant BMS phases associated with PGEs included pyrrhotite, chalcopyrite, and pentlandite. Pyrrhotite was the most common host, particularly in classes where PGEs were either associated with liberated BMS or with BMS attached to gangue. The primary modes of PGE occurrence in the BIC low-grade ore includes PtBiTe, PtFe, PtS and PtPdS (Fig. 12A, B and C). These results align with the well-documented behavior of PGEs in the BIC, where PGEs are generally found either bound to sulphides or in a liberated state.

## 5. Discussion

This study demonstrates the importance of integrating advanced mineralogical and geochemical analytical techniques for comprehensive ore characterisation. It also bridges the gap between rapid field-based (near real-time) analyses and detailed laboratory-based analysis by integrating HSI, pXRF, XRD and automated mineralogy. The implications of these results are significant for mineral exploration, processing optimisation, and sustainable resource management. The study shows the complementary nature of HSI, pXRF, and XRD in providing a multidimensional aspect of mineralogical and geochemical properties. The HSI perform rapid, non-destructive mineral identification based on

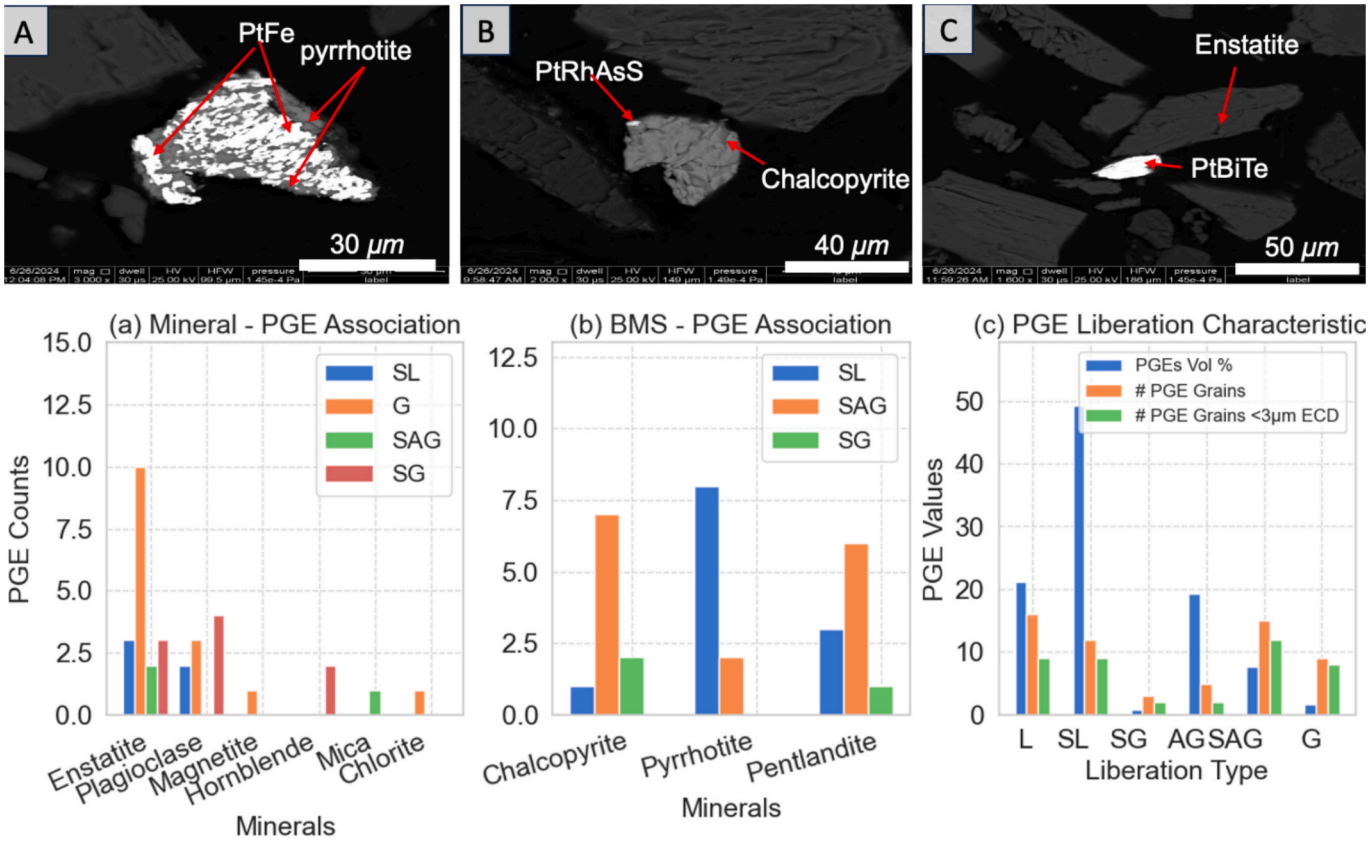


**Fig. 12.** Mineralogical microphotographs, mineral associations and PGE deportment as determined using MLA. L = liberated PGEs; SL= PGEs associated with liberated BMS; SG = PGEs associated with BMS locked in gangue; AG = PGEs attached to gangue; SAG = PGEs associated with BMS attached to gangue and G = PGEs locked in gangue minerals.

spectral features makes it helpful for large-scale drill core scanning, enabling efficient preliminary core assessments. However, HSI does not provide geochemical data. The pXRF quantifies elemental compositions which are important for determining ore grade and associating trace elements. XRD is used to confirm the definitive mineral phases and validate results from both HSI and pXRF.

The results show distinct mineralogical signatures corresponding to anorthosite (Fig. 3b; 4; Samples A and B) and norite (Samples C and D), which are consistent with BIC geology or lithologies. These results demonstrate the competency of the applied method to accurately delineate minerals and rock types. Therefore, the approach can help with improving geological mapping and guiding mineral exploration activities. This approach is particularly relevant in highly heterogeneous ore systems like the BIC, where precise mineralogical and geochemical data are important for identifying high-value zones and informing selective mining strategies. Comminution is important for mineral liberation and subsequent processing efficiency. A finer PSD, as observed in sample B (Fig. 7), improves mineral liberation by increasing ore surface area for better interaction with processing reagents (i.e., flotation and leaching). Conversely, a coarser PSD, as seen in sample A (Fig. 7), may retain unliberated valuable minerals, potentially reducing metal extraction rates.

Automated mineralogical analysis using TIMA and MLA provides important data into ore bulk mineralogy, PGE deportment and associations. TIMA results demonstrated that the ore mineralogy predominantly consists of pyroxene, feldspars and alteration (Fig. 8) with most BMS in free surface (Figs. 9, 10, 11). The connotation of enstatite and plagioclase as dominant gangue minerals associated with PGEs and BMS aligns with existing literature on the BIC (Gibson et al., 2023; Rose, 2016). The result from MLA shows that ~50 % of PGEs are associated with BMS, particularly pyrrhotite and ~20 % liberation of PGEs (Fig. 12). This information is important for developing metallurgical processes that target PGE-bearing sulphides. The observed mineral associations and PGE deportment allows for tailored beneficiation processes and improved metal recovery efficiencies. Understanding the dominance of sulphide-bound PGEs implies that flotation strategies should focus on improving the recovery of pyrrhotite and other BMS. The significant proportion of liberated PGEs presents opportunities for innovative recovery approach, such as gravity separation or direct leaching, which could complement flotation circuits.

The integration of HSI and pXRF in drill core (or ore) characterisation can improve the identification of high-grade zones, while XRD, TIMA and MLA provide detailed mineralogical insights to inform processing strategies. Mining operations can adopt selective mining practices, targeting ore zones with favourable mineralogical and geochemical characteristics by using these complementary techniques. Such an approach not only can improve extraction efficiencies but also minimises waste generation, contributing to sustainable resource utilisation. Although this study demonstrates the effectiveness of multi-technique analysis, further research is necessary to refine this integration. For example, (**1**) developing advanced machine learning algorithms to interpret HSI and pXRF data in real-time could improve the accuracy and speed of drill core analysis. (**2**) Expanding the study to include other sections of the BIC could validate the broader applicability of these methods. (**3**) Finally, investigating the impact of different milling and flotation conditions on PGE recovery from norite and anorthosite ores could provide deeper understanding into optimising beneficiation processes.

## 6. Conclusion

The integration of HSI, pXRF, XRD, MLA, and TIMA demonstrates the effectiveness of using complementary analytical instruments for ore characterisation. This multi-technique approach provides a clear understanding of mineralogical and geochemical compositions, enabling informed decision-making in exploration, processing, and resource utilisation optimisation. The combined use of these techniques can improve the accuracy of mineral identification, process efficiency and promote sustainable mining practices by optimising resource utilisation (or extraction) and reducing ore material losses. The PSD analysis is important in mineral liberation and subsequent ore processing. A finer PSD improves mineral liberation whereas coarser PSD may retain unliberated valuable minerals and potentially increase metal losses.

The correlation between geochemical and mineralogical datasets provides an ideal framework for ore characterisation and resource estimation. The integration of pXRF-derived geochemical data with mineralogy allows for a more precise delineation of sulphide-rich zones, improving exploration targeting and beneficiation strategies. BMS are known for their strong association with PGEs, therefore, they can serve as effective proxies for predicting PGE-rich zones, augmenting the efficiency of ore geometallurgical characterisation and resource modeling. The strong correlation of PGEs and base metals is shown in Fig. 6. The overall implication of this study is that a multi-technique approach is effective for accurate mineral characterisation and important for efficient resource utilisation. Integrating complementary analytical methods is promising to advance ore characterisation, beneficiation strategies, strengthens data driven decision-making in modern mining and improve geometallurgical advancements.

### 6.1. *Recommendation for future work*

It is recommended that more ore blocks be prepared and analysed using TIMA to increase the number of identified PGE grains and improve statistical robustness. Analysis on rock-prepared ore blocks is also suggested to confirm the inclusion of PGEs within BMS and better understand their deportment.

## Funding statement

This study was supported by the Wits Mining Institute through Mandela Mining Precinct, Mintek and Petroleum Agency of South Africa (PASA) Trust Fund (Upstream Training Trust).

## CRediT authorship contribution statement

**Viwe Notole:** Writing – review & editing, Writing – original draft, Visualization, Validation, Project administration, Methodology, Investigation, Formal analysis, Data curation, Conceptualization. **Glen T. Nwaila:** Writing – review & editing, Visualization, Validation, Supervision, Funding acquisition, Formal analysis, Conceptualization. **Mehdi Safari:** Writing – review & editing, Supervision, Funding acquisition, Conceptualization. **Sehliselo Ndlovu:** Writing – review & editing, Supervision, Conceptualization.

## Declaration of competing interest

The authors declare that they have no known competing financial interests or personal relationships that could have appeared to influence the work reported in this paper.

## Acknowledgements

The authors would like to thank the staff (Karin Greyling, Emil Burger, Prinushka Padiachy, and Richard Munyai) at Impala Bafokeng e, South Africa for providing us with samples used in this study. We would like to thank Council for Geoscience (Clement Ndou) for providing us with Hyperspectral scanning and assisting with analysis. . Finally, we would like to thank Mohau Rampou, Mintek mineral processing and mineralogy team for assisting with data analysis and mineralogy analysis.

## Data availability

Data will be made available on request.

## References


Amponsah-Dacosta, M., 2017. Mineralogical characterisation of South African mine tailings with aim of evaluating their potential for the purposes of mineral carbonation. M.Sc Thesis, University of Cape Town, South Africa. Available at: https://open.uct.ac.za/, (Accessed: 20 March 2025).

Aylmore, M.G., 2019. Automated mineralogy. SME Mineral Processing & Extractive Metallurgy Handbook; Dunne, RC, Kawatra, SK, Young, CA, Eds, pp.43-68.

Balaram, V., Sawant, S.S., 2022. Indicator minerals, pathfinder elements, and portable analytical instruments in mineral exploration studies. Minerals 12 (4), 394.

Barnes, S.J., Maier, W.D., Ashwal, L.D., 2004. Platinum-group element distribution in the main zone and upper zone of the Bushveld complex. South Africa. Chem. Geology 208 (1–4), 293–317.

Baloyi, N.P., Nheta, W., Sibanda, V., Safari, M., 2024. Mineralogical insights into PGM recovery from middle group (1–4) chromite tailings. Minerals 14, 924. https://doi.org/10.3390/min14090924.

Becker, M., Harris, P.J., Wiese, J.G., Bradshaw, D.J., 2009. Mineralogical characterisation of naturally floatable gangue in Merensky Reef ore flotation. Int. J. Miner. Process. 93 (3–4), 246–255.

Boudreau, A.E., 2008. Modeling the merensky reef, bushveld complex, republic of South Africa. Contrib. Miner. Petrol. 156, 431–446.

Buchspies, B., Thormann, L., Mbohwa, C., Kaltschmitt, M., 2017. PGE production in Southern Africa, part II: Environmental aspects. Minerals 7 (11), 225.

Cawthorn, R.G., 2015. The Bushveld Complex, South Africa. In: Layered intrusions. 2nd ed. Houghton Mifflin Harcourt, pp. 517-587.

Carelse, C., Manuel, M., Chetty, D., Taguta, J., Safari, M., Youlton, K., 2022. The flotation behaviour of liberated platinum Group minerals in Platreef ore under reduced reagent conditions. Miner. Eng. 190, 107913. https://doi.org/10.1016/j.mineng.2022.107913.

Chistyakova, S., Latypov, R., Youlton, K., 2019. Multiple merensky reef of the bushveld complex, South Africa. Contrib. Miner. Petrol. 174, 1–17.

Chistyakova, S.Y., Latypov, R.M., Kruger, F.J., Zaccarini, F., 2021. Transgressive nature and chilled margins of the Upper Zone in the western Bushveld complex. South Africa. the Canadian Mineralogist 59 (6), 1285–1303.

Cook, N.J., Ciobanu, C.L., Ehrig, K., Slattery, A., Verdugo-Ihl, M.R., Courtney-Davies, L., Gao, W., 2017. Advances and opportunities in ore mineralogy. Minerals 7 (12), 233.

Corin, K.C., McFadzean, B.J., Shackleton, N.J., O'Connor, C.T., 2021. Challenges related to the processing of fines in the recovery of platinum group minerals (PGMs). Minerals 11 (5), 533.

Cross, W., Iddings, J.P., Pirsson, L.V., Washington, H.S., 1902. A quantitative chemico-mineralogical classification and nomenclature of igneous rocks. J. Geol. 10 (6), 555–690.

Das, A.P., van Hullebusch, E.D., Akçil, A. (Eds.), 2024. Sustainable Management of Mining Waste and Tailings: A Circular Economy Approach. CRC Press.

Dominy, S.C., O'Connor, L., Parbhakar-Fox, A., Glass, H.J., Purevgerel, S., 2018. Geometallurgy—A route to more resilient mine operations. Minerals 8 (12), 560.

Ghorbani, Y., Zhang, S.E., Nwaila, G.T., Bourdeau, J.E., Safari, M., Hoseinie, S.H., Nwaila, P., Ruuska, J., 2023. Dry laboratories–Mapping the required instrumentation and infrastructure for online monitoring, analysis, and characterisation in the mineral industry. Miner. Eng. 191, 107971.

Gibson, B.A., Nwaila, G., Manzi, M., Ghorbani, Y., Ndlovu, S., Petersen, J., 2023. The valorisation of platinum group metals from flotation tailings: a review of challenges and opportunities. Miner. Eng. 201, 108216.

Gleason, J.D., Gutzmer, J., Kesler, S.E., Zwingmann, H., 2011. 2.05-Ga isotopic ages for transvaal mississippi valley–type deposits: evidence for large-scale hydrothermal circulation around the bushveld igneous complex, South Africa. J. Geol. 119 (1), 69–80.

Godel, B., Barnes, S.J., Maier, W.D., 2007. Platinum-group elements in sulphide minerals, platinum-group minerals, and whole-rocks of the Merensky Reef (Bushveld complex, South Africa): implications for the formation of the reef. J. Petrol. 48 (8), 1569–1604.

Hamann, R., 2004, November. Corporate social responsibility, partnerships, and institutional change: The case of mining companies in South Africa. In Natural resources forum (Vol. 28, No. 4, pp. 278-290). Oxford, UK: Blackwell Publishing Ltd.

Hayes, B., Maghdour-Mashhour, R., Ashwal, L.D., Smith, A.J., Ueckermann, H., Vermeulen, J., 2024. Melt infiltration in a crystal mush and pegmatoid formation in the platiniferous Merensky Reef, Bushveld complex. South Africa. Mineralium Deposita 1–23.

Hrstka, T., Gottlieb, P., Skala, R., Breiter, K., Motl, D., 2018. Automated mineralogy and petrology-applications of TESCAN Integrated Mineral Analyzer (TIMA). J. Geosci. 63 (1), 47–63.

Hu, C., Yang, Z., He, M., Zhan, Y., Zhang, Z., Peng, C., Zeng, L., Liu, Y., Yang, Z., Yin, H., Liu, Z., 2024. From waste to wealth: current advances in recycling technologies for metal recovery from vanadium-titanium magnetite tailings. J. Sustain. Metallurgy 1–29.

Hughes, A.E., Haque, N., Northey, S.A., Giddey, S., 2021. Platinum group metals: a review of resources, production and usage with a focus on catalysts. Resources 10 (9), 93.

Kinnaird, J.A., 2005. The Bushveld large igneous province. The University of the Witwatersrand, Johannesburg, South Africa, Review Paper, pp. 1–39.

Latypov, R., Chistyakova, S., Barnes, S.J., Hunt, E.J., 2017. Origin of platinum deposits in layered intrusions by in situ crystallization: evidence from undercutting Merensky Reef of the Bushveld complex. J. Petrol. 58 (4), 715–761.

Latypov, R.M., Namur, O., Bai, Y., Barnes, S.J., Chistyakova, S., Holness, M.B., Iacono-Marziano, G., Kruger, W.A., O'Driscoll, B., Smith, W.D., Virtanen, V.J., 2024. Layered intrusions: Fundamentals, novel observations and concepts, and controversial issues. Earth Sci. Rev. 249, 104653.

Lotter, N.O., 2011. Modern process mineralogy: an integrated multi-disciplined approach to flowsheeting. Miner. Eng. 24 (12), 1229–1237.

Maier, W.D., Barnes, S.J., Groves, D.I., 2013. The Bushveld complex, South Africa: formation of platinum–palladium, chrome-and vanadium-rich layers via hydrodynamic sorting of a mobilized cumulate slurry in a large, relatively slowly cooling, subsiding magma chamber. Miner. Deposita 48, 1–56.

Mashaba, D., 2022. An investigation into the complementary capabilities of X-ray computed tomography and hyperspectral imaging of drill core in geometallurgy. M. Sc Thesis, University of Cape Town, South Africa. Available at: https://open.uct.ac.za/, (Accessed: 20 March 2025).

Mayer, C.C., Jugo, P.J., Leybourne, M.I., Grobler, D.F., Voinot, A., 2021. Strontium isotope stratigraphy through the Flatreef PGE-Ni-Cu mineralisation at Turfspruit, northern limb of the Bushveld Igneous complex: evidence of correlation with the Merensky Unit of the eastern and western limbs. Miner. Deposita 56, 59–72.

McCall, M.J., 2016. Mineralogical and geochemical variations in the UG2 reef at Booysendal and Zondereinde mines, with implications for beneficiation of PGM (Doctoral dissertation. Stellenbosch University), Stellenbosch.

McCarthy, T., Rubidge, B., 2013. The story of earth & life: a southern african perspective on a 4.6-billion-year journey. Penguin Random House South Africa.

McDonald, I., Harmer, R.J., Holwell, D.A., Hughes, H.S., Boyce, A.J., 2017. Cu-Ni-PGE mineralisation at the Aurora Project and potential for a new PGE province in the Northern Bushveld Main Zone. Ore Geol. Rev. 80, 1135–1159.

McDonald, I., Holwell, D.A., 2011. Geology of the northern Bushveld complex and the setting and genesis of the Platreef Ni-Cu-PGE deposit. Miner. Deposita 46 (6), 649–674.

Mitra, S., 2019. Depletion, technology, and productivity growth in the metallic minerals industry. Miner. Econ. 32 (1), 19–37.

Mudd, G.M., Jowitt, S.M., Werner, T.T., 2018. Global platinum group element resources, reserves and mining–a critical assessment. Sci. Total Environ. 622, 614–625.

Mungall, J.E., Kamo, S.L., McQuade, S., 2016. U–Pb geochronology documents out-of-sequence emplacement of ultramafic layers in the Bushveld Igneous complex of South Africa. Nat. Commun. 7 (1), 13385.

Naldrett, A.J., Wilson, A., Kinnaird, J., Chunnett, G., 2009. PGE tenor and metal ratios within and below the Merensky Reef, Bushveld complex: implications for its genesis. J. Petrol. 50 (4), 625–659.

Naldrett, A.J., Wilson, A., Kinnaird, J., Yudovskaya, M., Chunnett, G., 2012. The origin of chromitites and related PGE mineralization in the Bushveld complex: new mineralogical and petrological constraints. Miner. Deposita 47, 209–232.

Naldrett, A.J., 2013. Magmatic sulfide deposits: geology, geochemistry and exploration. Springer Science & Business Media.

Nayak, A., Jena, M.S., Mandre, N.R., 2022. Beneficiation of lead-zinc ores–a review. Miner. Process. Extr. Metall. Rev. 43 (5), 564–583.

Nwaila, G.T., Frimmel, H.E., Zhang, S.E., Bourdeau, J.E., Tolmay, L.C., Durrheim, R.J., Ghorbani, Y., 2022. The minerals industry in the era of digital transition: an energy-efficient and environmentally conscious approach. Resour. Policy 78, 102851.

O'Connor, C., Alexandrova, T., 2021. The geological occurrence, mineralogy, and processing by flotation of platinum group minerals (PGMs) in South Africa and Russia. Minerals 11 (1), 54.

Osbahr, I., Klemd, R., Oberthür, T., Brätz, H., Schouwstra, R., 2013. Platinum-group element distribution in base-metal sulfides of the Merensky Reef from the eastern and western Bushveld complex, South Africa. Miner. Deposita 48, 211–232.

Oyinloye, C., 2024. The determination of separation characteristics and processability of REE minerals in X-Carbonatite ores (Master's thesis, C. Oyinloye).

Pebane, M., Latypov, R., 2017. The significance of magmatic erosion for bifurcation of UG1 chromitite layers in the Bushveld complex. Ore Geol. Rev. 90, 65–93.

Price, J., 2016. PGM Distribution and Reef Characterisation of the Merensky Reef at the Phosiri Dome, Bushveld Complex, South Africa. Master of Earth Sciences thesis, School of Earth & Ocean Sciences, Cardiff University, Cardiff, UK.

Prichard, H.M., Barnes, S.J., Maier, W.D., Fisher, P.C., 2004. Variations in the nature of the platinum-group minerals in a cross-section through the Merensky Reef at Impala platinum: Implications for the mode of formation of the reef. Can. Mineral. 42 (2), 423–437.

Roonwal, G.S., 2018. Mineral exploration: practical application, 1st ed. Springer, Cham.

Rose, D.H., 2016. A process mineralogical investigation of the merensky reef and Ug-2 at the two rivers platinum mine with emphasis on ore characterization. University of Johannesburg (South Africa).

Safari, M., Harris, M., Deglon, D., 2017. The effect of energy input on the flotation of a platinum ore in a pilot-scale oscillating grid flotation cell. Miner. Eng. 110, 69–74. https://doi.org/10.1016/j.mineng.2017.04.012.

Sahu, P., Jena, M.S., Mandre, N.R., Venugopal, R., 2021. Platinum group elements mineralogy, beneficiation, and extraction practices–An overview. Miner. Process. Extr. Metall. Rev. 42 (8), 521–534.

Schouwstra, R.P., Smit, A.J., 2011. Developments in mineralogical techniques–what about mineralogists? Miner. Eng. 24 (12), 1–12.

Schouwstra, R.P., Kinloch, E.D., Lee, C.A., 2000. A short geological review of the Bushveld complex. Platin. Met. Rev. 44 (1), 33–39.

Scoates, J.S., Wall, C.J., Friedman, R.M., Weis, D., Mathez, E.A., VanTongeren, J.A., 2021. Dating the Bushveld complex: timing of crystallization, duration of

magmatism, and cooling of the world's largest layered intrusion and related rocks. J. Petrol. 62 (2), g107.
Smith, G.L., 2011. A conceptual framework for the strategic long-term planning of platinum mining operations in the south african context. University of the Witwatersrand, Johannesburg, South Africa.
Smith, W., Maier, W., Barnes, S., Moorhead, G., Reid, D., Karykowski, B., 2021. Element mapping the merensky reef of the bushveld complex. Geosci. Front. 12 (3), 101101.
Taguta, J., Safari, M., Govender, V., Chetty, D., 2023. Investigating the amenability of a PGM-bearing ore to coarse particle flotation. Minerals 13 (5), 698. https://doi.org/10.3390/min13050698.
Verma, S.P., Torres-Alvarado, I.S., Velasco-Tapia, F., 2003. A revised CIPW norm. Swiss Bulletin of Mineralogy and Petrology 83 (2), 197–216.
Wills, B.A., Finch, J., 2015. Wills' mineral processing technology. Butterworth-Heinemann.
Wirth, R., Reid, D., Schreiber, A., 2013. Nanometer-sized platinum-group minerals (PGM) in base metal sulfides: New evidence for an orthomagmatic origin of the Merensky Reef PGE ore deposit, Bushveld complex. South Africa. the Canadian Mineralogist 51 (1), 143–155.
Zeh, A., Ovtcharova, M., Wilson, A.H., Schaltegger, U., 2015. The Bushveld complex was emplaced and cooled in less than one million years–results of zirconology, and geotectonic implications. Earth Planet. Sci. Lett. 418, 103–114.